



**HAL**  
open science

## **A Versatile Shaping Method of Very-High Loading Porous Solids Paper Adsorbent Composites**

Pierre Tignol, Vanessa Pimenta, Anne-Laurence Dupont, Silvia Carvalho, Abeer Al Mohtar, Maria Inês Severino, Farid Nouar, Moisés L Pinto, Christian Serre, Bertrand Lavédrine

► **To cite this version:**

Pierre Tignol, Vanessa Pimenta, Anne-Laurence Dupont, Silvia Carvalho, Abeer Al Mohtar, et al.. A Versatile Shaping Method of Very-High Loading Porous Solids Paper Adsorbent Composites. *Small Methods*, 2023, 2301343, 10.1002/smt.202301343 . hal-04346812

**HAL Id: hal-04346812**

**<https://hal.science/hal-04346812>**

Submitted on 15 Dec 2023

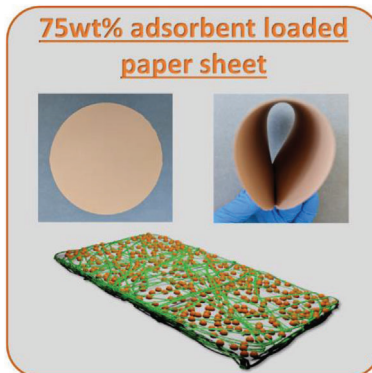
**HAL** is a multi-disciplinary open access archive for the deposit and dissemination of scientific research documents, whether they are published or not. The documents may come from teaching and research institutions in France or abroad, or from public or private research centers.

L'archive ouverte pluridisciplinaire **HAL**, est destinée au dépôt et à la diffusion de documents scientifiques de niveau recherche, publiés ou non, émanant des établissements d'enseignement et de recherche français ou étrangers, des laboratoires publics ou privés.

## RESEARCH ARTICLES

P. Tignol, V. Pimenta, A.-L. Dupont,  
S. Carvalho, A. A. Mohtar,  
M. Inês Severino, F. Nouar,  
M. L. Pinto, C. Serre,\*  
B. Lavédrine\* ..... 2301343

**A Versatile Shaping Method of  
Very-High Loading Porous Solids  
Paper Adsorbent Composites**



A green one-pot route combining two cellulosic products of different dimensions to prepare high-loading (>70 wt.%) porous solids (metal–organic frameworks, carbons, zeolites) paper sheets, with good flexural and strength mechanical resistance and preserved adsorption properties.

# A Versatile Shaping Method of Very-High Loading Porous Solids Paper Adsorbent Composites

Pierre Tignol, Vanessa Pimenta, Anne-Laurence Dupont, Silvia Carvalho, Abeer Al Mohtar, Maria Inês Severino, Farid Nouar, Moisés L. Pinto, Christian Serre,\* and Bertrand Lavédrine\*

Owing to their high porosity and tunability, porous solids such as metal–organic frameworks (MOFs), zeolites, or activated carbons (ACs) are of great interest in the fields of air purification, gas separation, and catalysis, among others. Nonetheless, these materials are usually synthesized as powders and need to be shaped in a more practical way that does not modify their intrinsic property (i.e., porosity). Elaborating porous, freestanding and flexible sheets is a relevant shaping strategy. However, when high loadings (>70 wt.%) are achieved the mechanical properties are challenged. A new straightforward and green method involving the combination softwood bleached kraft pulp fibers (S) and nano-fibrillated cellulose (NFC) is reported, where S provides flexibility while NFC acts as a micro-structuring and mechanical reinforcement agent to form high loadings porous solids paper sheets (>70 wt.%). The composite has unobstructed porosity and good mechanical strength. The sheets prepared with various fillers (MOFs, ACs, and zeolites) can be rolled, handled, and adapted to different uses, such as air purification. As an example of potential application, a MOF paper composite has been considered for the capture of polar volatile organic compounds exhibiting better performance than beads and granules.

allow them to interact specifically with a wide range of guest molecules (gases, vapors, liquids) making them appealing compounds of strong technological and scientific interest<sup>[1–3]</sup> in a large number of applications such as catalysis,<sup>[4]</sup> gas storage and separation,<sup>[5,6]</sup> sensing,<sup>[7]</sup> energy storage<sup>[8]</sup> and biomedicine.<sup>[9]</sup>

In the past few decades, in addition to the continuous development of mature materials such as activated carbons (ACs), zeolites, several new classes of porous solids have emerged among which metal–organic frameworks (MOFs), covalent–organic frameworks (COFs), and porous polymers are the most popular examples.<sup>[10]</sup> In most cases, these solids are produced in powder form and often require a shaping prior their practical use. Typical shaping methods consist in producing pellets and beads when associated with additives (solvent, binder) or specific process conditions (pressure, temperature), thereby requiring a case by case optimization

for each porous solid to meet the requirements of the targeted application.<sup>[13–15]</sup> Shaping may alter their intrinsic key sorption properties<sup>[11,12]</sup> and/or lead to irreversible textural and structural changes for instance upon application of an excessive mechanical

## 1. Introduction

Porous solids are highly versatile materials due to their exceptional structural and chemical tunability. These characteristics

P. Tignol, A.-L. Dupont, B. Lavédrine  
Centre de Recherche sur la Conservation  
Muséum National d'Histoire Naturelle  
CNRS  
Ministère de la Culture  
Paris 75005, France  
E-mail: bertrand.lavedrine@mnhn.fr

P. Tignol, V. Pimenta, M. Inês Severino, F. Nouar, C. Serre  
Institut des Matériaux Poreux de Paris  
EPCI Paris  
Ecole Normale Supérieure  
CNRS  
PSL University  
Paris 75005, France  
E-mail: christian.serre@ens.fr  
S. Carvalho, A. A. Mohtar, M. L. Pinto  
CERENA  
Departamento de Engenharia Química  
Instituto Superior Técnico  
Universidade de Lisboa  
Campus Alameda, Lisboa 1049-001, Portugal

 The ORCID identification number(s) for the author(s) of this article can be found under <https://doi.org/10.1002/smt.202301343>

© 2023 The Authors. Small Methods published by Wiley-VCH GmbH. This is an open access article under the terms of the Creative Commons Attribution-NonCommercial-NoDerivs License, which permits use and distribution in any medium, provided the original work is properly cited, the use is non-commercial and no modifications or adaptations are made.

DOI: 10.1002/smt.202301343

pressure,<sup>[16]</sup> or alternatively to the release of powder if the mechanical stability is insufficient.<sup>[17]</sup> Binders, on the other hand, can lead to a partial pore blocking and/or to strong diffusion limitations.<sup>[14]</sup>

To circumvent these shaping limitations, an alternative strategy is to produce flexible fiber-reinforced adsorbent layer sheets that can be cut to a specific size to suit the application such as gas adsorption,<sup>[18]</sup> water purification,<sup>[19]</sup> catalytic degradation<sup>[20]</sup> or biomedical applications.<sup>[21]</sup> Electrospinning is a simple, common technique which spins a blended porous solid/polymer suspension under a high voltage to form a stable, flexible and easy to handle freestanding composite.<sup>[22]</sup> Many synthetic polymers including polyacrylonitrile (PAN),<sup>[23]</sup> polystyrene (PS),<sup>[24]</sup> poly(vinylidene fluoride) (PVDF)<sup>[25]</sup> are generally used, leading to highly loaded porous solids composites (>70 wt.%).<sup>[26]</sup> However, this method often results in a reduced specific surface area due to the encapsulation of the porous solid particles by the polymer and/or the use of hazardous solvents DiMethylFormamide (DMF) that poison the pores of the adsorbent. As an alternative, other porous solid/fiber shaping strategies were developed such as solvent free hot-pressing<sup>[27,28]</sup> or textile fiber coating in aqueous/alcohol media.<sup>[29]</sup> However, this is limited to a given category of porous solids (MOFs), and lower porous solids loadings (<30 wt.%) are typically obtained, which calls for the development of new methods to prepare environmentally-friendly fiber-based composites that may be easily scalable. Those drawbacks lead us to investigate the use of cellulosic fibers as a binder for producing a paper sheet composite with high loading of porous solids.

Cellulose is the most abundant, natural and renewable biopolymer on earth with an annual biomass production of  $1.5 \times 10^{12}$  tons.<sup>[30]</sup> Cellulosic fibers have been combined with porous solids to produce filter papers with a high specific surface area for air or wastewater purification.<sup>[31–33]</sup> Such porous solids cellulosic composites can be prepared following two main routes: 1) in situ synthesis of porous particles in the presence of fibers and 2) ex situ blending where particles are mixed with the fibrous material. Some attempts have been recently reported with the direct growth of zeolites or MOFs on plant fibers.<sup>[34–36]</sup> For instance,  $\text{Cu}_3(\text{BTC})_2$  (BTC = 1,3,5-benzenetricarboxylate)<sup>[34]</sup> and  $\gamma$ -cyclodextrin-MOFs<sup>[35]</sup> have been synthesized in situ in the presence of plant fibers while zeolite A particles have been deposited on plant fibers through a similar route.<sup>[36]</sup> However, in both cases, the content of porous solids incorporated into the cellulosic substrate is as low as 5%, and cannot go beyond 40 wt.% without jeopardizing the mechanical stability of the composite due to the disruption of the fiber network at higher filler content.<sup>[37]</sup> The strength of a paper sheet depends not only on the fibers but also strongly relies on fiber-fiber interactions. The fillers content is usually kept ca. 20–35 wt.% to avoid a network per unit volume too low in fibers content, which ultimately reduces the strength of the paper.<sup>[38]</sup> Obtaining good mechanical stability at higher loading is therefore very challenging in terms of mechanical properties of the resulting composite paper sheet. Thus, another type of cellulose fiber, nanocellulose, has been used for its mechanical properties, which go far beyond those of conventional fibers.

Nano-fibrillated cellulose (NFC), also denoted cellulose nanofibers (CNFs), possesses a nanostructure with a high aspect ratio (nanometers wide and up to several micrometers long).<sup>[39]</sup>

It can be extracted from cellulose fibers by mechanical and/or chemical treatment and produced industrially at the tons per day scale.<sup>[40]</sup> Their high tensile stiffness and strength offers the possibility to form strong, as well as, complex composite materials.<sup>[41,42]</sup> They may increase the mechanical strength properties of paper by improving the fiber-fiber interactions.<sup>[43,44]</sup> Activated carbon (AC) in papers with a loading of 50–90 wt.%, prepared by ex situ blending with NFC, showed good mechanical properties (high tensile strength, i.e., 1.2 MPa for an AC paper sheet with a loading of 70 wt.%).<sup>[45]</sup> However, the formulation process includes multiple heating steps, while the flexural strength of the composite as well as its sorption properties were not studied. Other composites sheets have been reported based on 2,2,6,6-Tetramethylpiperidine-1-oxyl (TEMPO) oxidized cellulose nanofibers (TOCNF) with a high density of carboxyl groups at the surface.<sup>[46–48]</sup> Only a couple of examples using aqueous media for in situ synthesis and ex situ blending result in a high loading of porous solids (>70 wt.%).<sup>[49,50]</sup> For instance, the in situ synthesis route was applied to grow Zinc Imidazolate Framework (ZIF)-8, Universitetet i Oslo (UiO)-66(Zr), and Material from Institut Lavoisier (MIL)-53(Al) nanoparticles on TOCNF with a loading of 75–90 wt.%.<sup>[49]</sup> Zeolite (Zeolite Socony Mobil (ZSM)-5, silicalite-1, or Y) particles were alternatively mixed with TOCNF and polyethylene glycol (PEG) by ex situ blending with a zeolite loading of 60–97 wt.%, resulting in composites with high flexibility.<sup>[50]</sup> However, these procedures, although associated in most cases with high loadings and good mechanical properties, still suffer from significant drawbacks such as partial pore blockade, multiple and/or lengthy (days) formulation steps at the cost of high energy-demanding hydro- or solvo-thermal conditions. These downsides make these processes not environmentally-friendly and rule out their practical use at large scale. To the best of our knowledge, no green and economically viable procedure (Table S1, Supporting Information) has been reported so far to produce high-loading porous solids cellulosic-based composites, while ensuring both adequate sorption and good mechanical properties.

In this work, we report a versatile and green one-pot method that consists in combining cellulosic materials with different dimensions and aspect ratio, to prepare high loadings (>70 wt.%) porous solids paper sheets with unspoiled adsorption properties and good mechanical tensile and flexural properties. The cellulose sources are softwood bleached kraft pulp fibers (SBKP abbreviated S further on) and NFC that provide flexibility and tensile strength, respectively, resulting in a nanostructured paper-like non-powdery mesh with enhanced content of the porous solid particles. This low-energy, non-toxic, and straightforward process involves an energetic blend of the fibrous materials and the porous particles in water at room temperature, followed by a rapid filtering and drying steps (**Figure 1**). To demonstrate the feasibility and study the properties of such composite paper, heavily loaded sheets with the benchmark mesoporous Fe(III) trimesate MOF denoted MIL-100(Fe) were prepared by varying several parameters such as MOF content, S:NFC ratio and pH. The structure of those sheets was studied through powder X-ray diffraction (PXRD), infrared spectroscopy (IR), thermal gravimetric analysis (TGA), nitrogen porosimetry, optical microscopy (OM), scanning electron microscopy (SEM) and 3D X-Ray microscopy. The mechanical properties were assessed using coaxial tensile strength

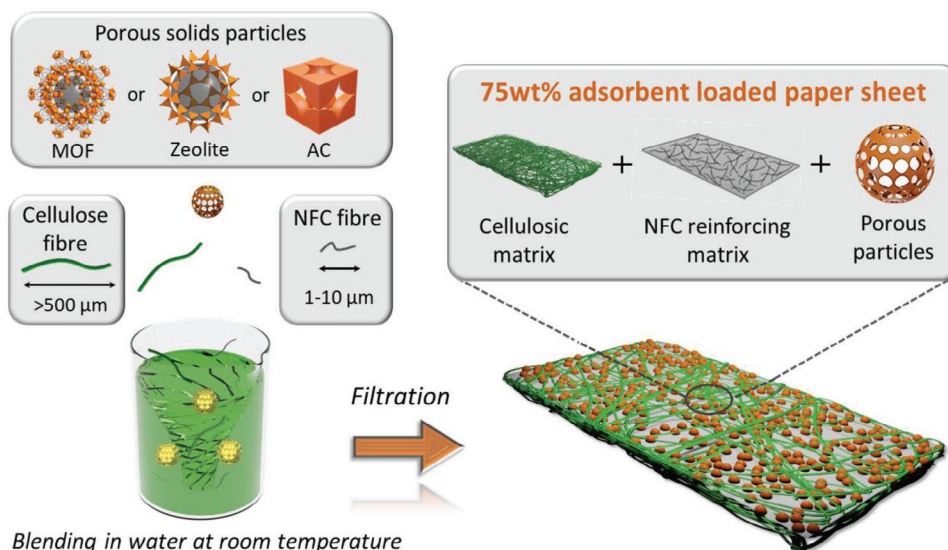


**Figure 1.** Scheme illustrating the green preparation process of the sheet containing different porous solids (Activated Carbon (AC), metal–organic framework (MOF), Zeolite) combined with an NFC-reinforced cellulosic matrix.

and bending tests measurements. After optimizing the quality of the sheets and shedding light on the interaction mechanisms involved, this easily scalable route was applied to produce 75% MIL-100(Fe) sheets with other MOFs, as well as commercial zeolite and activated carbon. As an example of application, such sheets were tested for a polar VOC, e.g. acetic acid capture that is a common but deleterious VOC for cultural goods.<sup>[51,52]</sup> As will be demonstrated in the following, the MIL-100(Fe) paper sheet exhibited equal performance to that of the MIL-100(Fe) powder and significantly outperformed other mechanically-shaped products traditionally used in adsorption-related applications. This demonstration allows to envisage broader application fields, such as large volume indoor air purification or moisture control.

## 2. Results and Discussion

### 2.1. MIL-100(Fe) Composite Paper Sheet

A paper sheet was prepared with 75 wt.% MIL-100(Fe) embedded in a cellulose matrix composed of softwood fibers (S) and nano-fibrillated cellulose (NFC) (more details provided in the Experimental Section). MIL-100(Fe) that exhibits mesoporous cages (25 and 29 Å) accessible through microporous windows (5.7 and 8.2 Å)<sup>[53]</sup> was selected for the paper sheet optimization due to: 1) its biocompatibility, green, and scalable synthesis<sup>[54,55]</sup> and 2) its physico-chemical properties (mesoporosity, hydrolytic stability, Lewis acid or redox active sites) of interest for a wide range of possible applications such as thermochemical energy,<sup>[56,57]</sup> water purification,<sup>[58,59]</sup> catalysis,<sup>[60,61]</sup> gas storage,<sup>[62,63]</sup> and biomedicine,<sup>[64,65]</sup> among others. To reach the ambitious target of a 75 wt.% loading of MIL-100(Fe) in a paper sheet with sufficient mechanical stability, we have also considered two distinct particle sizes for MIL-100(Fe): microparticles (1 to 2 microns, Figure S1, Supporting Information), denoted “microMOF”, and nanoparticles (few hundred nanometers as aggregates, Figure S2, Supporting Information), denoted

“nanoMOF” both prepared through a simple ambient pressure route as reported previously (further details in Supporting Information).<sup>[55,66,67]</sup>

Figure 2a shows a paper sheet (ca. 20 cm in diameter) made of a mixture of S and NFC (25:75 ratio), and containing 75 wt.% of nanoMOF. Note that the sheet could easily be made larger or smaller, in agreement with its simple and scalable preparation route. It is also significantly flexible (Figure 2b). SEM image analysis indicates that the components are homogeneously distributed as shown on a cross-section that exhibits a dense packing structure with a thickness of about 350 µm (Figure 2c). The PXRD pattern of the composite is also in good agreement with the one of MIL-100(Fe), simulated and experimental (Figure 2d), indicating that the ambient conditions formulation process does not decrease the crystallinity of the MOF. The Fourier transform infrared (FTIR) spectra (Figure 2e; Figure S3, Supporting Information) further confirm that the nanoMOF and the corresponding paper sheet exhibit similar main characteristic asymmetric and symmetric stretching bands: carboxylate groups at 1630–1577 and 1448–1379 cm<sup>-1</sup> (Figure 2e) as well as trimeric Fe<sub>3</sub>O sub-unit at 620 cm<sup>-1</sup> (Fe–O bond).<sup>[66]</sup> The slight differences between the powder and the composite lie in the 900 and 1200 cm<sup>-1</sup> regions where cellulose bands are found: at 1160 cm<sup>-1</sup> this corresponds to the asymmetric C–O–C vibration while those at 1031 and 1053 cm<sup>-1</sup> are attributed to the C–C bond of the pyranose ring (Figure 2f).<sup>[68]</sup> Thermogravimetric analyses under oxygen atmosphere were first conducted on nanoMOF (Figure 2g), S and NFC separately (Figure S4, Supporting Information). The nanoMOF shows three weight losses corresponding to: 1) desorption of free solvent molecules from the pores ( $T < 100$  °C), 2) removal of bound water molecules (100–250 °C) and 3) decomposition of the ligand at higher temperature (300 °C).<sup>[69]</sup> S and NFC both exhibit an initial weight loss (>90 wt.%) until 150–200 °C due to the loss of physisorbed water prior to the onset of thermal decomposition at ca. 280 °C. S degrades completely between 280 and 310 °C whereas NFC degrades between 280 and 450 °C. This

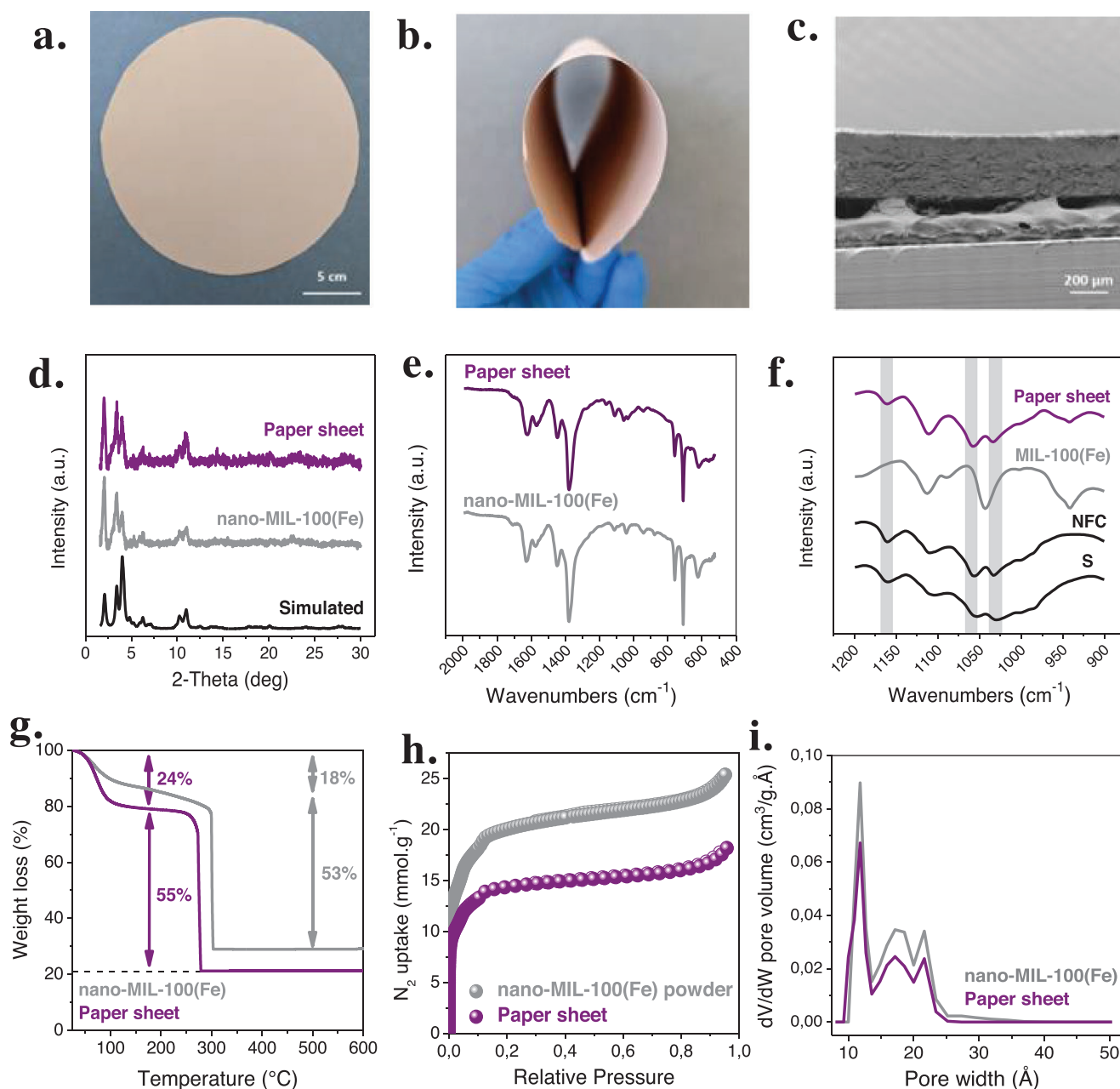


**Figure 2.** a) 75 wt.% nano-MIL-100(Fe) paper sheet (cellulosic matrix = softwood bleached kraft pulp and NFC, ratio 25:75). b) Image showing the flexibility of the nano-MIL-100(Fe) paper sheet. c) SEM image of the cross-section of the sheet. d) PXRD patterns of simulated, nano-MIL-100(Fe) as powder and 75 wt.% MIL-100(Fe) paper sheet ( $\text{Cu-K}\alpha$ ,  $\lambda = 1.5406 \text{ \AA}$ ). e) FTIR spectra of nano-MIL-100(Fe) as powder and in 75 wt.% paper sheet in the range  $500\text{--}2000 \text{ cm}^{-1}$ . f) FTIR spectra of S, NFC, nano-MIL-100(Fe) as powder and in 75 wt.% paper sheet in the range  $900\text{--}1200 \text{ cm}^{-1}$ . g) TGA of nano-MIL-100(Fe) and 75 wt.% paper sheet. h)  $\text{N}_2$  adsorption–desorption isotherms obtained at 77 K (adsorption, filled symbols; desorption, empty symbols) of nano-MIL-100(Fe) as powder and the corresponding paper sheet. i) Pore size distribution (PSD) of nano-MIL-100(Fe) as powder and the corresponding paper sheet.

is attributed to their slightly different compositions since S contains less thermally stable substances such as hemicelluloses and few residual lignin,<sup>[70]</sup> prior to their conversion mainly into  $\text{CO}_2$ ,  $\text{H}_2\text{O}$ , and  $\text{CO}$  molecules.<sup>[71]</sup> The nanoMOF based paper sheet (Figure 2g) exhibits a thermal behavior similar to the one of the raw materials, being stable up to  $280 \text{ }^\circ\text{C}$ . The major weight loss of the composite (55 wt.%) combines the degradation of the fibers

and the MOF ligand, ultimately forming iron oxide  $\text{Fe}_2\text{O}_3$ . In addition, TGA enabled to estimate the MIL-100(Fe) content to about 72 wt.%.  $\text{N}_2$  porosimetry at 77 K was conducted on the nanoMOF and the composite sheet (Figure 2h). The porosity of the composite leads to a BET specific surface area close to  $1245 \pm 18 \text{ m}^2 \text{ g}^{-1}$  versus  $1720 \pm 20 \text{ m}^2 \text{ g}^{-1}$  for the nanoMOF. This is consistent with the percentage of MOF introduced ( $\approx 75 \text{ wt.}\%$ ) considering

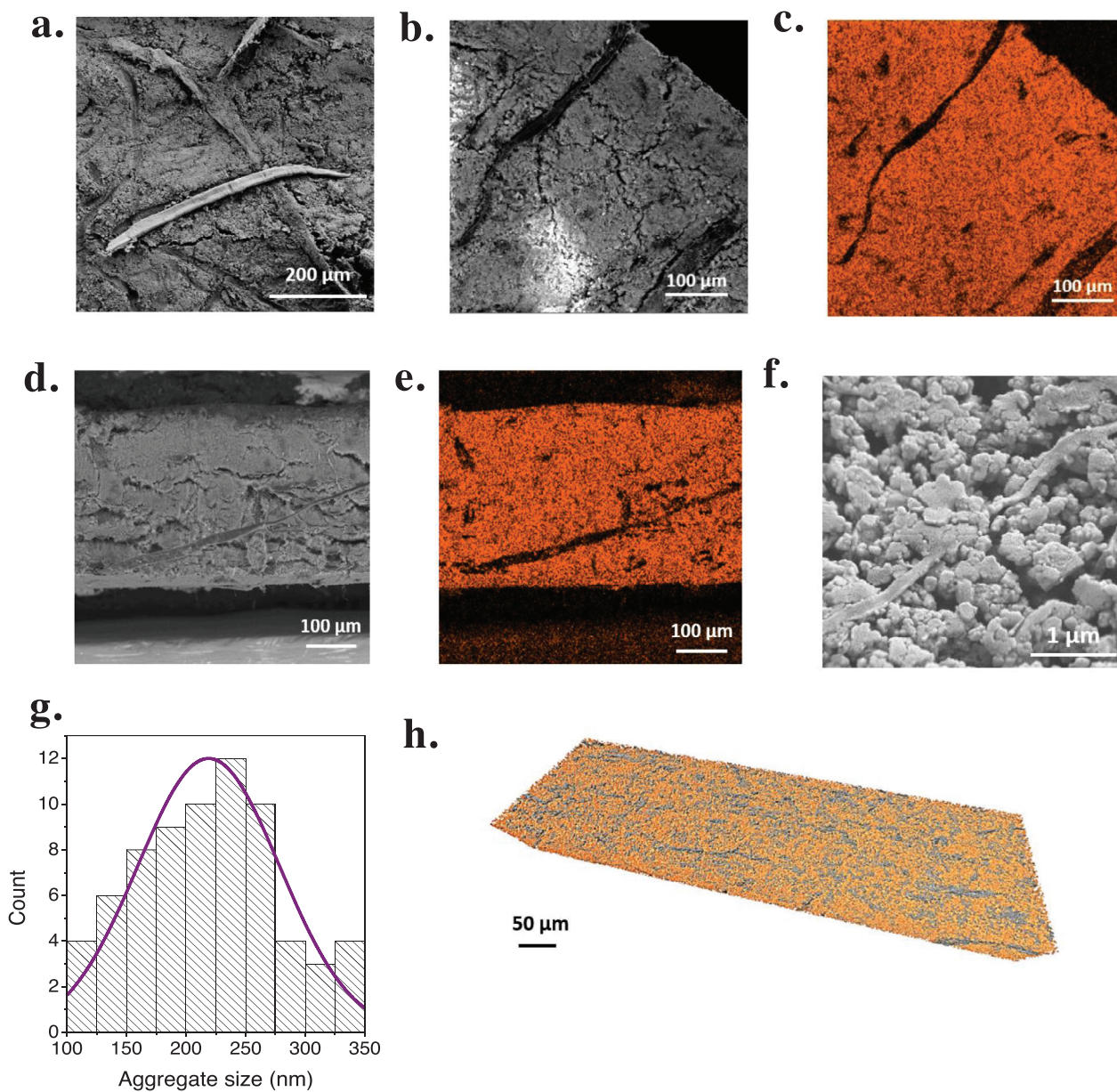


**Figure 3.** a) SEM image of 75 wt.% nano-MIL-100(Fe) paper sheet 25S-75NFC at a magnification of about 884 $\times$  (scale bar = 200  $\mu\text{m}$ ). b–e) SEM observation of the paper with a,b) flat (scale bar = 100  $\mu\text{m}$ ) and c,d) cross-section (scale bar = 200  $\mu\text{m}$ ). Panels (c,e) are the EDX elemental maps of iron (Fe) in the 75 wt.% nano-MIL-100(Fe) paper sheet 25S-75NFC observed: b,c) flat (scale bar = 100  $\mu\text{m}$ ) and d,e) cross-section (scale bar = 100  $\mu\text{m}$ ). f) SEM image of 75 wt.% nano-MIL-100(Fe) paper sheet 25S-75NFC at magnification of 151 000 $\times$  (scale bar = 1  $\mu\text{m}$ ). g) Histogram representing the aggregate size distribution of nano-MIL-100(Fe) in the paper sheet using Image J software. h) 3D model of the 75 wt.% micro-MIL-100(Fe) paper sheet (cellulosic matrix in grey and micro-MOF in orange) based on the CT scanning data.

that S and NFC contribute with negligible surface area, and confirming that the porosity of the MOF is fully preserved once in the paper sheet. Pore size distribution (PSD) estimated by DFT calculation (Figure 2i) present peaks at 11.8, 17.2, and 21.4  $\text{\AA}$  for nanoMOF, corroborating the presence of micro/mesopores, showing little differences for the paper sheet. A sheet was prepared with microMOF (75 wt.%) and yielded a paper composite of similar quality, highlighting the robustness of the formulation and preparation method (details in, Figure S5, Supporting Information).

Micro- and nano-MIL-100(Fe) paper sheets were observed by SEM. S fibers of several hundred microns up to a few millimeters can be identified (Figure 3a; Figures S6 and S7a, Supporting Information), with a homogeneous distribution of MOF particles on the surface and throughout the cross-section, as evidenced by Fe elemental mapping (Figure 3b–e; Figure S7a–d, Supporting Information). At higher magnification (Figure 3f; Figure S7e, Supporting Information), the NFC is clearly visible. It appears in the form of small fibers of a few microns in length, dispersed with no preferential orientation. In the nanoMOF paper sheet, the

nanoparticles are aggregated, with an average size of  $220 \pm 60$  nm due to the limited colloidal stability of the nanoMOF (Figure 3g). This is confirmed through dynamic light scattering (DLS) where the hydrodynamic radius (aggregates surrounded by a diffuse layer) in aqueous solution is  $570 \text{ nm} \pm 140$  (at a concentration of  $0.1 \text{ g L}^{-1}$ ). On the other hand, the MIL-100(Fe) microparticles are individually identified with an average size estimated at  $1.5 \pm 0.4 \mu\text{m}$  (Figure S7f, Supporting Information). The microstructure of the paper sheets was further studied using 3D X-ray microscopy by computed tomography (CT-scan). CT-scan observations of the nanoMOF paper sheet revealed a few discrete particles, agglomerated on the surface of the fibers (Video S1, Supporting Information named NanoMIL100; ). However, since the resolution was limited by the size of the MOF particles, a better observation was achieved with the microMOF paper sheet. The microMOF particles are homogeneously distributed in the volume (Figure S8a, Supporting Information) and throughout the thickness (grey/white shading) with voids (black background) suggesting a macroporosity in the sample (Figure S8b, Supporting Information) which may favor gas diffusion (bulk density =  $0.275 \text{ g cm}^{-3}$ ). A reconstructed 3D model (Figure 3h) shows the spatial organization of the cellulosic matrix and microMOF particles throughout the volume, confirming the dense packing structure of the sheet as observed by SEM (Figure S7c,d, Supporting Information). A second short movie depicts the 3D structure where MOF particles and NFC can be observed as small dots while S is observed as long fibers, when moving the cutting plane through the sample (Movie S2, Supporting Information; named MicroMIL100-full).

## 2.2. Impact of the MOF Content

To assess the influence of the nanoMOF content over the paper sheet properties, we first kept the same S to NFC ratio 25:75 and tuned the MOF relative ratio between 60 and 90 wt.%. TGA indicates an average MOF loading of 61, 72, and 90 wt.%, respectively (Figure S9, Supporting Information) and the porosity of the composites (Figure S10, Supporting Information) is once again well correlated with the amount of loaded MOF, ranging from  $S_{\text{BET}}$  of  $1090 \pm 15$ ,  $1245 \pm 17$  to  $1550 \pm 20 \text{ m}^2 \text{ g}^{-1}$ , respectively (Table S2, Supporting Information), with little Particle Size Distribution (PSD) differences compared to the nanoMOF (Figure S11, Supporting Information). In order to assess the impact of the MOF ratio on the mechanical properties of the sheet, coaxial tensile strength measurements were performed (Figure S12, Supporting Information). The tensile strength measurements show that an increase of the MOF loading in the composite leads to a significant decrease of the tensile strength, Young modulus and a lower strain. Although the ultimate tensile strength (UTS), corresponding to the maximum stress that a material can endure when pulled before breaking, drops from 3 MPa to 1.5 MPa for the 60 and the 75 wt.% MOF paper sheet, respectively, both sheets can still easily be handled without creasing. However, when the loading reaches 90 wt.%, the UTS of the paper sheet falls to less than 0.5 MPa, which results in a sheet too brittle for easy handling and practical use. Similarly, the strain decreases linearly with the increase of the nanoMOF loading. The fibers content plays a significant role on the mechanical strength of the composite due to

strengthening role of the inter-fiber interactions. Comparatively, Li et al obtained better mechanical properties for TOCNF composite with 90 wt.% ZIF-8 grown in situ<sup>[49]</sup> or TOCNF/PEG composites loaded with 90 wt.% zeolites (ZSM-5, silicalite-1 or Y) with 2 and 6–10 MPa in tensile strength, respectively.<sup>[50]</sup> However, in both cases, a considerable loss of porosity from 20 to 40% was observed in those cases based on the BET surface areas calculations, due to a partial pore blocking and/or problem in the activation steps with possible degradation of PEG at high temperatures ( $T > 80 \text{ }^\circ\text{C}$ ). In addition, both procedures<sup>[49,50]</sup> involved multi-steps, lengthy conditions or the use of hazardous solvents (DMF, methanol). The simple, ambient and green route proposed in our work enables the optimal of 75 wt.% MOF loading paper that ensures sufficient mechanical stability and a high porosity without pore blocking.

## 2.3. Optimization of the Cellulosic Fibers to NFC Ratio

In order to further optimize the 75 wt.% nano-MIL-100(Fe) paper sheet by tuning the cellulosic matrix content, the S:NFC ratio was varied as follow: 100:0, 75:25, 50:50, 25:75, 10:90, and 0:100. PXRD patterns (Figure S13, Supporting Information) and FTIR analyses (Figures S14, S15, Supporting Information) are in line with those of the previous nanoMOF paper sheets. In TGA profiles (Figure S16, Supporting Information), it is interesting to note that in the composites where the cellulose content is 100% S, the MOF content is lower than expected. Indeed, the nanoMOF loading in the paper sheet with 100% S is  $\approx 64$  wt.% without NFC (100S) to  $\approx 71$ –73 wt.% with NFC (25 to 100%). This is probably due to a partial loss of particles during the filtration process into the filtrate and/or adhering to the filter. The MIL-100(Fe)–100S composites therefore have a powderier aspect as shown by the residue on the adhesive tape after adhering to the sheets (Figure S17, Supporting Information). This is in line with NFC enhancing the cohesion of the composite by acting as a micro-structuring agent. Its addition enhances intermolecular bonds with MOF particles and concomitantly improves inter-fiber bonding due to the increased number of fiber-fiber interactions,<sup>[37]</sup> resulting into a complex network with a better accommodation of MOF particles and the fibers.  $N_2$  porosimeter shows, as previously, that the porosity of the composites is maintained (Figures S18 and S19, Supporting Information) with surface areas ( $S_{\text{BET}}$ ) of NFC based nanoMOF composites ranging from  $1235 \pm 15$  to  $1245 \pm 18 \text{ m}^2 \text{ g}^{-1}$  (Table S4, Supporting Information), respectively. In agreement with TGA analysis, the composites without NFC (100% S) exhibit a lower porosity and therefore a lower BET surface area (Tables S3, Supporting Information).

In order to assess the impact of the cellulosic matrix composition on the mechanical properties, coaxial tensile strength measurements were performed (Figure 4a). The stress–strain curves evolve gradually depending on the percentage of NFC in the cellulose matrix, indicating that the ultimate tensile strength (UTS) and Young's modulus are improved by the addition of NFC in the composites made of nanoparticles (Figure S20, Supporting Information). When containing only S, the composite is more brittle (UTS < 0.4 MPa and Young modulus < 100 MPa). However, remarkably, upon addition of a small proportion of

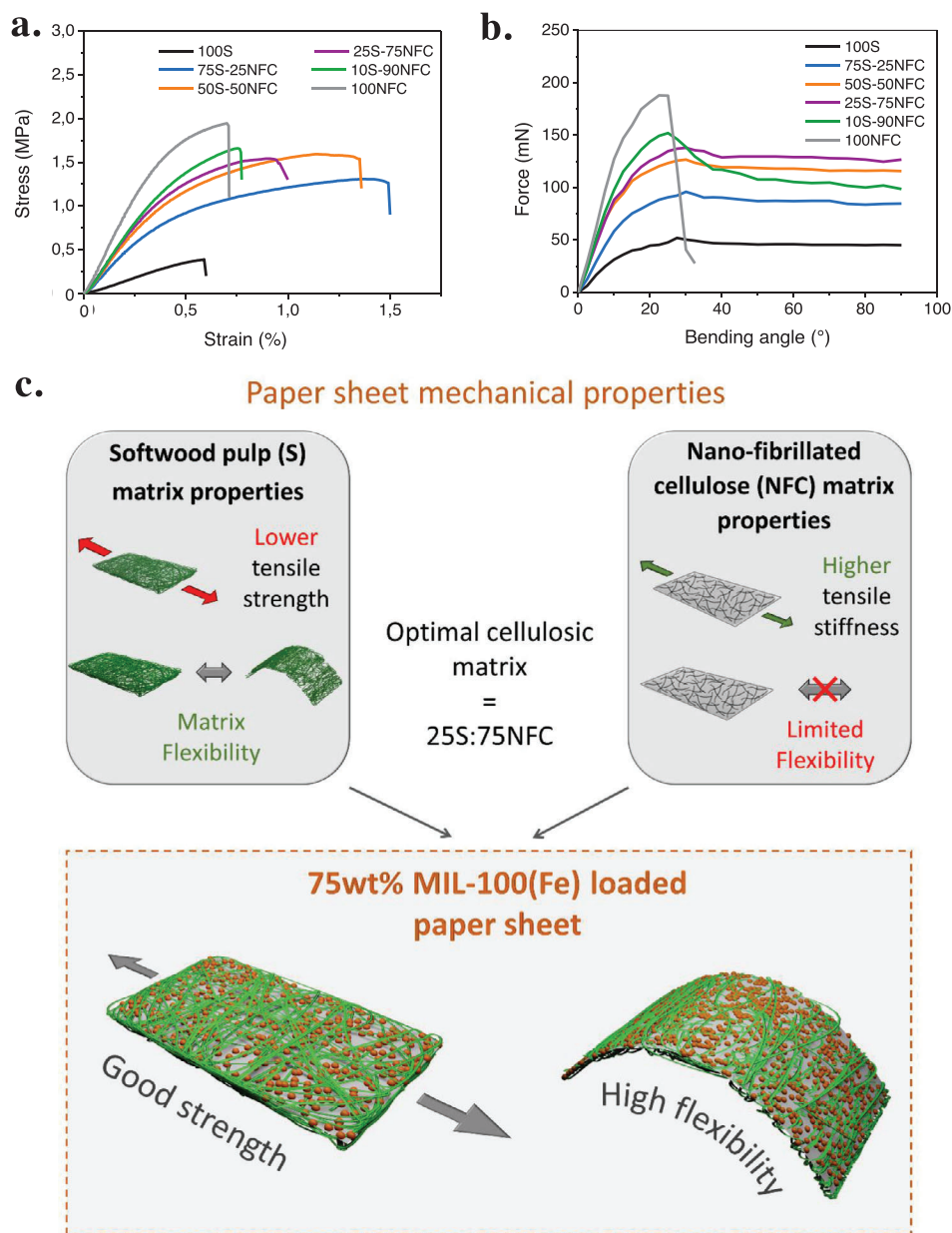


**Figure 4.** a) Strain–stress curves of 75 wt.% nano-MIL-100(Fe) paper sheets made with different cellulosic matrices. b) Force versus angular deflection of the paper sheets containing different cellulosic matrix investigated by two-point method to deduce the flexibility of the 75 wt.% nano-MIL-100(Fe) paper sheets. c) Scheme highlighting the benefits of combining two different cellulosic matrices to produce a paper sheet consisting of 75 wt.% MIL-100(Fe) with good mechanical properties.

NFC (75S:25NFC) both the UTS and related Young modulus triple. Consequently, the paper sheet becomes less brittle and easier to handle. When the cellulose matrix contains only NFC (100NFC), the UTS reaches 2 MPa for composites made of 75 wt.% nanoparticles, where the bare NFC film has a UTS higher than 150 MPa.<sup>[72]</sup> Two-point bending tests were carried out to analyze the flexible character and the flexural strength of the composites (Figure 4b). The curves force versus bending angle shows a linear portion, corresponding to the elastic regime up to an angle of  $\approx 20^\circ$  followed by a plastic deformation (i.e., same constant force at higher angles) for the composites. One can therefore point out that a higher proportion of NFC corre-

lates well with a higher bending force, as confirmed by the calculated bending stiffness (Figure S21, Supporting Information). In contrast, when composites contain only NFC (100NFC), they break at a bending angle of about  $20^\circ$  (with very little plastic deformation) suggesting that S plays a decisive role in the flexibility of the paper sheets. Cross-sections of the 75 wt.% MIL-100(Fe) loaded papers after the flexibility tests were observed with SEM (Figure S22, Supporting Information) and showed no cracking or major differences compared to the initial samples (Figure 2c, 3d). The optimization of the S:NFC ratio carried out with micro-MOF following the same procedure as with nanoMOF, indicated the same optimal ratio, 25S:75NFC (details in Figures S23–S33,

Table S4, Supporting Information). Based on these observations, a scheme is tentatively proposed to describe the synergetic effect of the two types of cellulosic fibers to form high MOF-loading paper sheets with enhanced mechanical properties (Figure 4c). The best compromise between flexibility and tensile strength of the paper sheets is obtained with the ratio S:NFC = 25:75 (Figure 4) and corresponds to the folded 75 wt.% MIL-100(Fe) paper sheets shown in Figure 2b; Figure S5b (Supporting Information). This cellulosic materials proportion was thus selected for further experiments.

## 2.4. Influence of pH on MIL-100(Fe) Paper Sheets

To obtain a better insight of the influence of the pH on the paper composite, Zeta potential measurements of the individual components were carried over the pH range of 2.5–6.5 (Figure S34, Supporting Information). Up to about pH 3.5, MIL-100(Fe) particles are positively charged and become negatively charged above this pH. NFC being negatively charged over the whole pH range due to possible residual cellulose and hemicellulose carboxyls,<sup>[68]</sup> a pH below 3.5 would enhance the electrostatic attraction between the NFC and the MOF particles. When preparing the paper composite, and before filtration, the pH of the suspension containing the fibers/particles mixture was quite acidic probably due to the partial deprotonation of trimesic carboxylic acids ( $pK_a$ s = 3.16, 3.98, and 4.85) on the surface of the particles (pH2.5 for the nanoparticles).<sup>[73]</sup> However, cellulose is known to degrade when in contact with acids.<sup>[74,75]</sup> This is due to the acid-catalyzed hydrolysis reaction which cleaves the glycosidic bonds in cellulose and hence leads to a decrease in the degree of polymerization (DP),<sup>[76]</sup> which in turn leads to a decrease in the mechanical properties of paper.<sup>[75,77]</sup> In addition, both the MOF particles and the cellulosic fibers exhibit a specific charge – pH behavior that might impact the overall stability of the sheet: at pH 6 both NFC fibers and MOF particles have a negative surface charge causing possible electrostatic repulsions (Figure S34, Supporting Information). To better characterize this, the impact of the pH of the suspension MOF/cellulose on the mechanical properties of the composite was studied. This also helped shedding light on the possible interactions within the composite between the fibers and the MOF particles. The pH of nanoMOF suspensions was first increased to pH 6 by adding a few drops of diluted aqueous NaOH solution ( $C = 10^{-3}$  M) prior to adding the MOF particles to form 75 wt.% MIL-100(Fe) composite (cellulosic matrix S:NFC = 25:75). Nitrogen porosimetry carried out before and after the pH adjustment at 77 K indicated no significant differences between the composites (i.e., same porosity) (Figures S35 and S36a, and Table S5, Supporting Information). Tensile strength measurements (Figure S37a, Supporting Information) were performed and showed a slight improvement of the UTS and Young's modulus for micro- and nanocomposites prepared at pH 6 in comparison with the sheets prepared under more acidic conditions (Figure S37b–d, Supporting Information). The flexural behavior was assessed and showed that the flexural stiffness was improved to a similar level for the nano-scale MIL-100(Fe) paper sheets prepared at pH 6 (Figure S38, Supporting Information). The same pH effect was observed with microMOF paper sheets (Figures S35–S38, Table S5, Supporting

Information). In general, an acidic environment leads to a drop in the DP of the cellulose and consequently a drop in the paper's tensile strength (more details in Supporting Information).<sup>[77]</sup> In our case, this indicates that when in suspension in an acidic pH solution, the DP, and hence the mechanical properties of the composite, can be impacted by the fibers' degradation. Despite the change in surface charges at pH 6 (promoting electrostatic repulsions), the composites exhibit better mechanical properties than those prepared from suspensions at acidic pH. This indicates that the electrostatic interactions play a minor role in the mechanical properties of the composite and that, as in paper, the dominant forces are more likely to be hydrogen bonds between fibers.

## 2.5. Extension to Other Porous Solids

As the strategy was initially optimized using the benchmark MOF MIL-100(Fe), it was interesting to assess whether the methodology could be generalized to other adsorbents with different structural and chemical features (pore size, composition, particle aspect ratio). For the preparation of 75 wt.% porous solids composites relying on a cellulose matrix with a 25S-75NFC ratio, we selected hydrophobic adsorbent such as i) MIL-53(Al)-CF<sub>3</sub>, a microporous perfluorinated Al 1,4-benzenedicarboxylate MOF synthesized in water under reflux (more details given in the experimental section) of interest for the capture of polar VOCs<sup>[79]</sup> (Figure S39, Supporting Information), and ii) a commercial activated carbon (Figure S40, Supporting Information), as well as, for the sake of comparison, the hydrophilic zeolite NaY (Figure S41, Supporting Information). The particles size and shape depend on the nature of the adsorbent (Figure 5a–f). In the case of MIL-53(Al)-CF<sub>3</sub>, the rod-like particles are relatively monodispersed and aggregated with an average size of  $190 \pm 50$  nm while for NaY consists of larger octahedral particles of  $700 \pm 115$  nm. Activated carbon is more polydisperse with randomly shaped particles ranging from a few microns to almost 100 microns. A similar preparation method as for the MIL-100(Fe) sheets was followed in all cases. Remarkably, all sheets are visually smooth and homogeneous (Figures S42 and S43, Supporting Information) with good flexibility (Figure 5g–i). All characterizations (PXRD, FTIR, TGA, N<sub>2</sub> adsorption/desorption) showed no impact on the structural and adsorption properties of the adsorbents (Figures S39–S41, Supporting Information; Table 1). Even if a case-by-case optimization would be needed for each sorbent, in a preliminary approach, this demonstrates that the simple preparation route developed enables the one-pot, rapid, green production of high-quality paper sheets with good mechanical properties with a large range of porous solids. Note that all these paper sheets (Figure S44, Supporting Information) are stable in water, with no defibrillation or particle shedding.

## 2.6. Application to the Capture of Polar Volatile Organic Compounds (VOCs)

As a preliminary attempt to assess the adsorption performances of the paper sheet, acetic acid (AcOH) was selected as a representative example of polar VOC that is challenging to capture

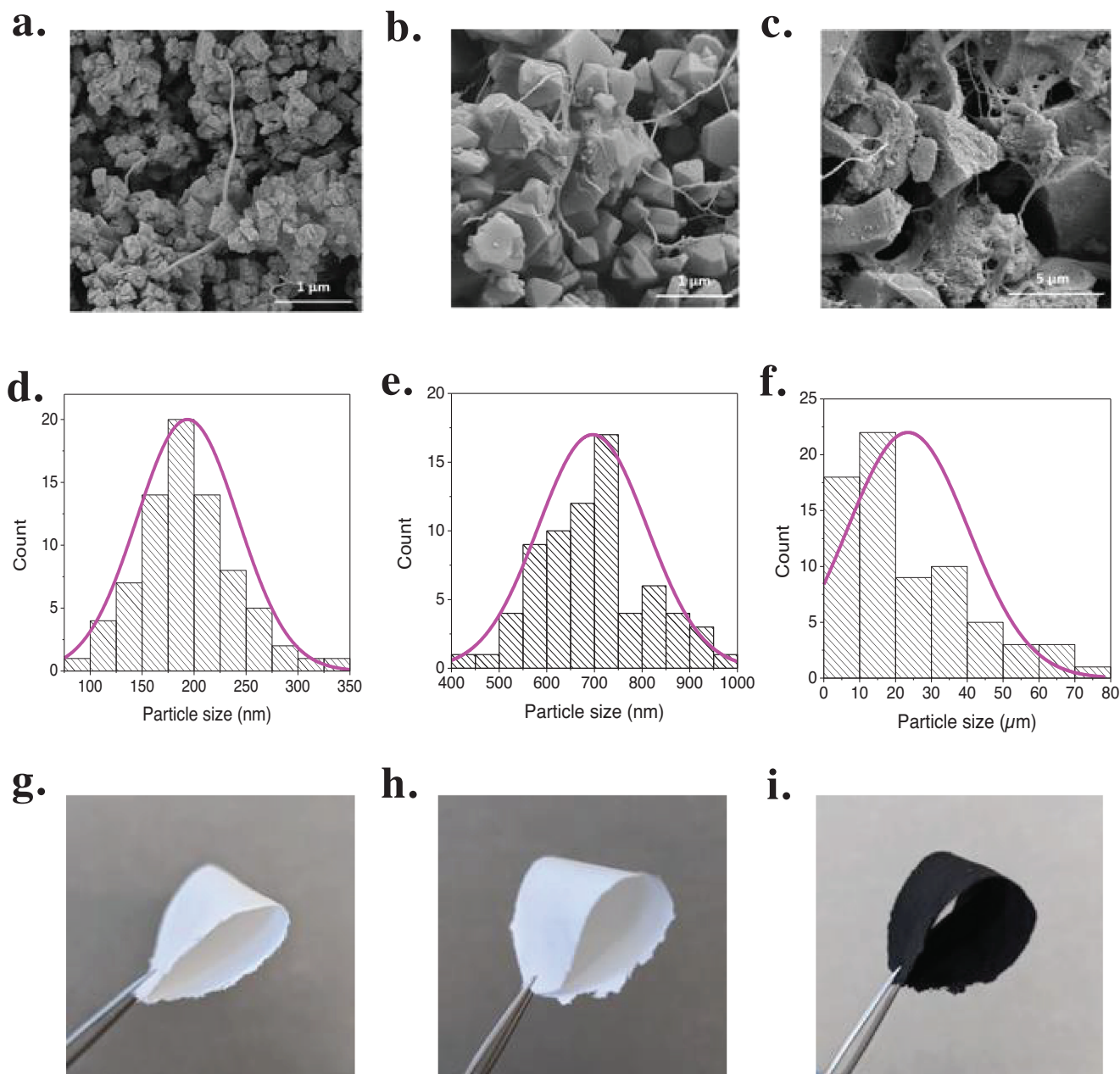


**Figure 5.** 75 wt.% paper sheets SEM pictures (at different magnification) made with: a) MIL-53(Al)-CF<sub>3</sub> (34 300×, scale bar = 1 μm), b) Zeolite NaY (34 300×, scale bar = 1 μm), and c) Activated carbon (8380×, scale bar = 5 μm). Histograms representing the particle size distribution of: d) MIL-53(Al)-CF<sub>3</sub>, e) Zeolite NaY, and f) Activated carbon in the paper sheets using Image J software. Images showing the flexibility of the 75 wt.% paper sheets made with: g) MIL-53(Al)-CF<sub>3</sub>, h) Zeolite NaY, and i) Activated carbon.

using adsorbents due to the strong competitive adsorption with water. It has been recently demonstrated that MOFs bearing open metal(III) sites (OMS) such as MIL-100(Fe) are capable to selectively capture AcOH even in the presence of humidity through a chemisorption mechanism involving their Lewis acid sites.<sup>[55]</sup> This is of strong interest to museums, libraries, and archives, to better preserve heritage objects that are sensitive to acid vapors (metal, ceramic, limestone, glass, among others) as well as emissive objects such as cellulose acetate-based artifacts by protect-

ing them from auto-catalytic degradation.<sup>[80]</sup> The use of an adsorbent paper composite offers many advantages for this application, where the use of powdery or powdery materials presents risks of contamination or soiling of artifacts.

The optimized 75 wt.% micro-MIL-100(Fe) paper sheet was first tested for the capture of AcOH. A purpose-made set-up was used to carry out the tests using a photoionization detector (PID) connected to a humid air (35–50% relative humidity) test chamber ( $V = 0.5 \text{ dm}^3$ ) where AcOH (1 μL) was injected,

**Table 1.** Textural parameters of different porous solids as powder and the corresponding 75 wt.% paper sheets.

Sample	$S_{\text{BET}}$ [ $\text{m}^2 \text{g}^{-1}$ ]	$V_{\text{pore}}$ [ $\text{cm}^3 \text{g}^{-1}$ ]
MIL-53(Al)- $\text{CF}_3$	$765 \pm 3$	0.35
MIL-53(Al)- $\text{CF}_3$ paper	$565 \pm 2$	0.27
Zeolite NaY	$860 \pm 2$	0.32
Zeolite NaY paper	$620 \pm 1$	0.23
Activated carbon	$1500 \pm 2$	1.18
Activated carbon paper	$1150 \pm 2$	0.88

corresponding to AcOH partial pressure  $P/P_0$  of about 0.027 in the chamber (more details in, Figure S45, Supporting Information) and a maximal concentration comprised between 480 and 560 ppm (Figure S46, Supporting Information). The mass of sheet inserted into the chamber was set to 3.5 mg (more details given in Supporting Information) and a constant time of 1.5 h was chosen. The AcOH concentrations detected in the chamber were the same after 1.5 h and one night incubation, confirming that the maximum level of adsorption of the paper sheet was reached. No change in the MOF/fiber microstructure after AcOH exposure was observed by SEM (Figure S47, Supporting Information) as well as a negligible impact on the mechanical properties (Figure S48, Supporting Information). The adsorption capacity is approximately  $4.1 \text{ mmol AcOH g}^{-1}$  of paper sheet, similar to that obtained with nano-MOF ( $4 \text{ mmol}_{\text{AcOH}} \text{g}^{-1}_{\text{paper}}$ ). The higher the MOF loading of the paper, the greater the AcOH adsorption capacity, increasing from 3.3 to  $4.8 \text{ mmol}_{\text{AcOH}} \text{g}^{-1}_{\text{paper}}$  for 60 and 90 wt.% nano-MOF loaded papers, respectively (Figure S49, Supporting Information). Furthermore, the MOF paper sheet could be easily regenerated by a simple soaking in water at room temperature after which the same adsorption capacity for AcOH was fully recovered ( $4.1 \text{ mmol}_{\text{AcOH}} \text{g}^{-1}_{\text{paper}}$ , Figure S50, Supporting Information).

## 2.7. MOF Shaping Effect on Adsorption Properties

To better evaluate the impact of MOF shaping on the adsorption properties, the AcOH adsorption isotherm of the 75 wt.% MIL-100(Fe) loaded paper sheet was compared to the ones of the traditional MOF beads containing 85–95 wt.% of MIL-100(Fe) made by wet granulation using different inorganic or organic binders (characterizations in Figure S51, Supporting Information). Noteworthy, at a  $P/P_0$  below 0.05, which corresponds to the binding of the AcOH on the open metal sites, the AcOH isotherms at  $25^\circ\text{C}$  (Figure S52, Supporting Information) showed that only the paper sheet exhibits a performance identical to the powder, while performing much better than the granules and the beads. These results confirm that the shaping as a paper sheet does not alter the physicochemical properties of the MOF, while the mechanical shaping using various binders most likely is associated with a partial poisoning of the OMS. In a second step, the adsorption behaviors of MIL-100(Fe) as powder, paper sheet and beads/granules were compared using a different environmental chamber set-up (Figure S53, Supporting Information), that simulates the conservation storage boxes used in the cultural heritage sector, as previously reported by Dedecker et al.<sup>[81]</sup> As shown be-

fore, the MIL-100(Fe) powder is highly efficient to reduce the concentration of AcOH from 80 ppm (injected dose) to 13 ppm after 1.5 h of exposure (Figure S54, Supporting Information). Remarkably, the MOF paper sheet lowered the concentration further to 7 ppm (contribution of the cellulosic matrix), while the beads and granules were much less effective, with AcOH concentrations between 20 and 27 ppm, in agreement with a lower accessibility of the OMS to capture AcOH.

Finally, the impact of the shaping on the pressure drop was assessed (Figure S55, Supporting Information). An excessive pressure drop in air purification systems is usually associated with a higher energy penalty and thus shall be minimized. The use of binders to shape porous solids is a well-known strategy to enhance the gas diffusivity but excessive pore blocking or lack of interparticular meso/macroporosity hamper their practical use if the pressure drop is too excessive. Here, the MOF paper sheet exhibits a minimal pressure drop in comparison with a commercial paper filter, indicating a fast diffusion of gas species. All these results confirm the excellent adsorption properties of MOF paper sheet, which can be easily used, for example, for indoor air quality and/or humidity control in buildings.

## 3. Conclusion

In this work, we developed a straightforward, rapid, green, scalable, and versatile route for the preparation of high-content porous solids paper sheets (>70 wt.%). This new preparation route in water at room temperature involved a combination of two cellulose fibers with an order of magnitude size difference, i.e., softwood bleached kraft pulp fibers that provide flexibility to the composite and NFC nanofibers with high tensile strength that act as microstructuring material, confer mechanical reinforcement and retain the smallest sorbent particles. This synergistic effect of the two cellulose-based materials led to mechanically stable composite paper sheets with, for the first time, very high adsorbent loading of 75 wt.% without compromising their intrinsic adsorption properties, even outperforming those of traditional shaped particles such as beads. Noteworthy not only this method does not require any specific particle size distribution for the adsorbent, but was also shown to be applicable to different classes of porous solids whatever their structural and chemical features, from MOFs, zeolites, or activated carbons. Such an unprecedented, versatile, green, and scalable route paves the way for the integration of high-loading porous solids paper sheets into a wide range of potential applications, from gas phase separation, heat allocation, sensing, biomedicine, among others.

## 4. Experimental Section

**Materials:** All chemicals were used without further purification. 1,3,5-Benzenetricarboxylic acid, 98% (Alfa Aesar), 2-(Trifluoromethyl)-1,4-benzenedicarboxylic acid (Angene), Acetic acid glacial, 100% (Supelco), Activated charcoal (Fisher Scientific), Aluminium chloride hexahydrate, 98% (Alfa Aesar), Bentonite (Sigma-Aldrich), Ethanol absolute anhydrous (Carlo Erba reagents), Iron fine powder (Riedel-de Haën), Iron nitrate monohydrate, 98% (Sigma-Aldrich), Nanofibrillated cellulose (Celova, Weidmann), Nitric acid 65% (Carlo Erba reagents), Pural (Sasol, high purity alumina with 74%  $\text{Al}_2\text{O}_3$  and 16% MgO), Silica (Sigma-Aldrich, 30 wt.% colloidal silica solution), Sodium hydroxyde pellets, 98% (Alfa

Aesar), Softwood pulp (HWBK, Canson), Zeolite Y, sodium 5.1 SiO<sub>2</sub>:Al<sub>2</sub>O<sub>3</sub> (Alfa Aesar).

**MOFs Synthesis:** MIL-100(Fe) microparticles and nanoparticles (Fe<sub>3</sub>O[C<sub>6</sub>H<sub>3</sub>-(CO<sub>2</sub>)<sub>3</sub>]<sub>2</sub>·OH·nH<sub>2</sub>O) as well as MIL-53(Al)-CF<sub>3</sub> nanoparticles (Al(OH)(C<sub>6</sub>H<sub>3</sub>CF<sub>3</sub>C<sub>2</sub>O<sub>4</sub>)) were synthesized in water. Detailed protocols were given in Supporting Information.

**Softwood:NFC Ratio Adjustment in 75 wt.% MIL-100(Fe) Paper Sheet:** X<sub>5</sub> g (X<sub>100</sub> = 0.874 g, X<sub>75</sub> = 0.656 g, X<sub>50</sub> = 0.437 g, X<sub>25</sub> = 0.218 g or X<sub>0</sub> = 0 g) (Table S6, Supporting Information) of softwood bleached kraft pulp (S) were dispersed using a blades blender in 1 L of distilled water and then redispersed in 4 L of distilled water and stirred. Y<sub>NFC</sub> g (Y<sub>0</sub> = 0 g, Y<sub>25</sub> = 0.218 g, Y<sub>50</sub> = 0.437 g, Y<sub>75</sub> = 0.656 g or Y<sub>100</sub> = 0.874 g) (Table S6, Supporting Information) of nano-fibrillated cellulose (NFC) gel at a concentration of 3 wt.% in water was added to the mixture. Then, 2.622 g of MIL-100 micro or nanoparticles (mass adjusted according to the amount of solvent contained in the pores) were placed in 250 mL of distilled water and placed in an ultrasonic bath for 15 min (resulting pH of micro and nano-MIL-100(Fe) solutions was respectively 3.5 and 2.5). The solution was added to the cellulosic mixture and left stirring for 15 min. The suspension was then filtered under vacuum using a Rapid Köthen handsheet former machine. The resulting 20 cm diameter paper sheet was dried under vacuum at 85 °C for 30 min using a dryer attached to the handsheet machine. The resulting composite contains 75 wt.% of MIL-100(Fe).

**Evolution of MIL-100(Fe) Percentage in the Paper Sheet:** The same protocol as above was followed but changing the percentage of MIL-100(Fe) (nanoparticles) to 60 and 90 wt.% while keeping the sheet mass constant (m = 3.496 g) and the cellulosic matrix ratio 25S:75NFC (Table S7).

**Fixing the pH of MIL-100(Fe) Paper Sheets:** The same protocol as above was used with 0.218 g softwood pulp and 0.656 g NFC (S:NFC ratio = 25:75). In contrast, the pH of the nano-MIL-100(Fe) and micro-MIL-100(Fe) solutions was adjusted to 6 by adding dropwise a solution of NaOH (C = 10<sup>-3</sup> M). The resulting 20 cm paper composites contain 75 wt.% MIL-100(Fe).

**Preparation of 75 wt.% Paper Sheets with Various Porous Solids:** A 31.25 mg of softwood pulp (HWBK, bleached kraft pulp) was inserted into a blade mill with 30 mL of distilled water for 2 min. A further 30 mL was added to this suspension. The resulting fiber mixture was dispersed during 5 min using an ultrasound probe (it was also possible to work in a larger volume of water to eliminate this step). A total of 93.75 mg of NFC were added to the fiber suspension and the mixture was stirred for 15 min. Three hundred seventy-five milligrams of porous solid such as MIL-53(Al)-CF<sub>3</sub>, zeolite NaY, and activated carbon particles were dispersed in an ultrasonic bath in 10 mL of distilled water (or ethanol in the case of MIL-53(Al)-CF<sub>3</sub>) for 10 min. The suspension was added to the fiber suspension and kept under stirring for 15 min (300 rpm). The mixture was filtered under vacuum, pressed with a mold pressing machine, and dried at room temperature resulting in 7 cm diameter paper sheets.

**Preparation of Nano-MIL-100(Fe) Based Mechanical Shaped Composites with Various Binders (Silica, Bentonite, and Pural):** Granules with 85–95 wt.% nano-MIL-100(Fe) loading were prepared by granulation and extrusion process. The protocol is fully detailed in Supporting Information.

**Characterizations:** Crystal structure of the porous solids was carried out by powder X-ray diffraction (XRD) using a Bruker Advance D8 diffractometer equipped with a copper source (CuKα radiation λ<sub>Cu</sub> = 1.5406 Å), at room temperature, in air. Transmission Infra-Red spectra were measured with a Nicolet iS5 spectrometer in a range from 500 to 4000 cm<sup>-1</sup>. Thermogravimetric analysis was performed under O<sub>2</sub> using a Model Mettler Toledo TGA/DSC2, STAR system. The samples (approximately 10 mg of each) were heated at a rate of 5 °C min<sup>-1</sup> up to 600 °C (or 700 °C when needed). N<sub>2</sub> adsorption-desorption isotherms were measured at 77 K with a TriStar II apparatus using a liquid nitrogen cryogenic bath. The samples were activated under primary vacuum using a Micromeritics degasser overnight at temperatures between 150 and 200 °C. Surface topography of the samples was performed by scanning electron microscopy using an ultra-high resolution Tescan Clara. The spatial distribution of MOF and NFC particles was carried out by 3D X-Ray microscopy using a nano-CT SkyScan 2214, Bruker equipped with an X-Ray tube (Tungsten source) and a CCD detector system (voltage = 110 kV, current = 180 μA, rota-

tion step = 0.15, number of frames 2401, exposure time = 2000 ms, voxel size = 0.5 μm). The reconstruction of the CT was done using the NRecon software (version 2.1.0.0, Bruker) based on the Feldkamp algorithm. CTAn software (version 1.18.8.0, Bruker) was used for the 3D analysis. A region of interest (ROI) representative of the sample was selected and, the images were binarized. The objects of interest were represented in white color. The quantitative analyses of the sample were then performed through the 3D plug-in analysis. CTvox software (Bruker) (version 3.3.0, Bruker) was used for volume rendering. Zeta-potential was investigated using a Malvern Zetasizer Nano-ZS, nano-MIL-100(Fe) and NFC aqueous suspensions were prepared at 3 wt.%. Mechanical properties were carried out by tensile strength measurements using an Adamel Lhomargy tensile machine (DY20-N, 100 dN load cell). Each sample had a length of 10 cm and a width of 1.5 cm. The distance between the jaws was 5 cm with an elongation rate of 50 mm.min<sup>-1</sup> and a breakage detection set at 3%. The samples were preconditioned for at least 24 h at 25 °C and 50% relative humidity and the tests were carried out under the same conditions. The measurement was repeated on 5 samples each. The flexibility of the paper sheets was studied using a two-point bending resistance tester (Büchel Van Der Korput). Each sample had a length of 5 cm and a breadth of 3.8 cm. The samples were preconditioned at least one day at 23 °C and 50% relative humidity and the tests were carried out under the same conditions. The measurement was repeated on 3 samples each. All bending stiffness calculations were performed according to ISO5628:2019.

**Volatile Organic Compound Capture Tests:** The first set-up and detailed steps are described in Supporting Information. Briefly, the experiment consists in injecting 1 μL of acetic acid into a glass chamber (V = 0.5 dm<sup>3</sup>), then measuring AcOH vapor concentrations after 1 h 30 min using a PID (ppbRAE 3000+, Honeywell). In the presence of an adsorbent, the steps are identical but the composite (75 wt.% micro-MIL-100(Fe), m = 3.5 mg) is first inserted into the chamber. The area covered by the VOC concentration versus time curve during the purge represents the amount of AcOH present in the vessel. These optimized experimental parameters were then used to compare the adsorption properties of paper sheets consisting of 60, 75, and 90 wt.% nano-MIL-100(Fe) (m = 3.5 mg). The 75 wt.% micro-MIL-100(Fe) loaded paper sheet was regenerated by soaking in distilled water for two days, changing water twice a day. The composite was then activated under vacuum at 150 °C overnight. The regenerated composite (m = 3.5 mg) was tested again in the environmental chamber with an exposure time of 1.5 h.

AcOH adsorption isotherms of MIL-100(Fe) powder, MIL-100(Fe) paper (75 wt.% loading) and MIL-100(Fe) beads (85–95 wt.% loading) were carried out using a microbalance (CI Electronics) equipped with a pressure sensor (capacitance manometer MKS a-BARATRON, 10 Torr range) at a controlled temperature of 25 °C (VMR, VWB2 series, 0.2 °C temperature stability).

The second setup consists of a larger glass chamber (V = 2.9 dm<sup>3</sup>) with a PID placed inside. This test measured AcOH concentrations in real time. Measurements were performed with 50 mg of MIL-100(Fe) as powder and MIL-100(Fe) shaped as paper composite (75 wt.% loading) or as granules (85–95 wt.% loading) with different binders (silica, bentonite, or pural) after injecting 1 μL of AcOH (more details provided in Supporting Information).

## Supporting Information

Supporting Information is available from the Wiley Online Library or from the author.

## Acknowledgements

This work was funded by the European Union's Horizon 2020 research and innovation program under grant agreement No 760801\Nemosine, and by Fundação para a Ciência e a Tecnologia (FCT) in the scope of the projects UIDB/04028/2020 & UIDP/04028/2020 (CERENA). The authors thank Karine Janel, Nathalie Marlin, Gérard Mortha, and Jérémie

Vigüé from INP Grenoble, for helping prepare the 20 cm paper sheets and perform the mechanical flexibility tests at Pagora (LGP2, UMR5518); to Stéphane Bouvet and Eléonora Pelizzi at Bibliothèque Nationale de France (BNF) for access to the tensile testing equipment; to Sabrina Paris Lacombe for help in obtaining the right conditions for the tensile strength measurements; to Georges Mouchaham for helping to draw porous solids structures on Diamond at ESPCI (IMAP, UMR8004); to Weidmann for providing free samples of NFC.

## Conflict of Interest

The authors declare no conflict of interest.

## Data Availability Statement

The data that support the findings of this study are openly available in ChemRxiv at 10.26434/chemrxiv-2023-h7g51-v2, reference number 0.

## Keywords

adsorption, cellulose, metal organic frameworks, NFC, paper sheets, porous solids

Received: October 12, 2023  
Published online:

- [1] X.-Y. Yang, L.-H. Chen, Y. Li, J. C. Rooke, C. Sanchez, B.-L. Su, *Chem. Soc. Rev.* **2017**, 46, 481.
- [2] M.-H. Sun, S.-Z. Huang, L.-H. Chen, Y. Li, X.-Y. Yang, Z.-Y. Yuan, B.-L. Su, *Chem. Soc. Rev.* **2016**, 45, 3479.
- [3] M. E. Davis, *Nature* **2002**, 417, 813.
- [4] J. Liang, Z. Liang, R. Zou, Y. Zhao, *Adv. Mater.* **2017**, 29, 1701139.
- [5] R. E. Morris, P. S. Wheatley, *Angew. Chem., Int. Ed.* **2008**, 47, 4966.
- [6] R.-B. Lin, S. Xiang, W. Zhou, B. Chen, *Chem* **2020**, 6, 337.
- [7] D. J. Wales, J. Grand, V. P. Ting, R. D. Burke, K. J. Edler, C. R. Bowen, S. Mintova, A. D. Burrows, *Chem. Soc. Rev.* **2015**, 44, 4290.
- [8] W. Li, J. Liu, D. Zhao, *Nature Rev. Mater.* **2016**, 1, 16023.
- [9] P. Horcajada, R. Gref, T. Baati, P. K. Allan, G. Maurin, P. Couvreur, G. Férey, R. E. Morris, C. Serre, *Chem. Rev.* **2012**, 112, 1232.
- [10] J. R. Holst, A. I. Cooper, *Adv. Mater.* **2010**, 22, 5212.
- [11] U. Mueller, M. Schubert, F. Teich, H. Puetter, K. Schierle-Arndt, J. Pastré, *J. Mater. Chem.* **2006**, 16, 626.
- [12] B. Valizadeh, T. N. Nguyen, K. C. Stylianou, *Polyhedron* **2018**, 145, 1.
- [13] G.-P. Hao, W.-C. Li, D. Qian, G.-H. Wang, W.-P. Zhang, T. Zhang, A.-Q. Wang, F. Schüth, H.-J. Bongard, A.-H. Lu, *J. Am. Chem. Soc.* **2011**, 133, 11378.
- [14] R. Bingre, B. Louis, P. Nguyen, *Catalysts* **2018**, 8, 163.
- [15] A. Permyakova, O. Skrylnyk, E. Courbon, M. Affram, S. Wang, U.-H. Lee, A. H. Valekar, F. Nouar, G. Mouchaham, T. Devic, G. De Weireld, J.-S. Chang, N. Steunou, M. Frère, C. Serre, *ChemSusChem* **2017**, 10, 1419.
- [16] D. Bazer-Bachi, L. Assié, V. Lecocq, B. Harbuzaru, V. Falk, *Powder Tech.* **2014**, 255, 52.
- [17] X.-M. Liu, L.-H. Xie, Y. Wu, *Inorg. Chem. Front.* **2020**, 7, 2840.
- [18] J. Zhao, B. Gong, W. T. Nunn, P. C. Lemaire, E. C. Stevens, F. L. Sidi, P. S. Williams, C. J. Oldham, H. J. Walls, S. D. Shepherd, M. A. Browe, G. W. Peterson, M. D. Losego, G. N. Parsons, *J. Mater. Chem.* **2015**, 3, 1458.
- [19] H.-W. Liang, X. Cao, W.-J. Zhang, H.-T. Lin, F. Zhou, L.-F. Chen, S.-H. Yu, *Adv. Funct. Mater.* **2011**, 21, 3851.
- [20] S. F. Anis, A. Khalil, Saepurahman, G. Singaravel, R. Hashaikhe, *Microporous Mesoporous Mater.* **2016**, 236, 176.
- [21] J. Chen, Z. Huang, H. Zhang, Z. Zhang, D. Wang, D. Xia, C. Yang, M. Dong, *Chem. Eng. J.* **2022**, 443, 136234.
- [22] Y. Dou, W. Zhang, A. Kaiser, *Adv. Sci.* **2020**, 7, 5785.
- [23] M. J. Soberman, L. Wang, D. Jia, W. Xia, J. Li, Z. Guo, *Sep. Purif. Technol.* **2020**, 253, 117461.
- [24] Y. Zhang, S. Yuan, X. Feng, H. Li, J. Zhou, B. Wang, *J. Am. Chem. Soc.* **2020**, 138, 5785.
- [25] D. Kang, H. Kang, *Appl. Surf. Sci.* **2016**, 387, 82.
- [26] J. Xiong, A. Li, Y. Liu, L. Wang, X. Qin, J. Yu, *J. Mater. Chem.* **2021**, 9, 37.
- [27] A. Wang, R. Fan, X. Zhou, S. Hao, X. Zheng, Y. Yang, *ACS Appl. Mater. Interfaces* **2018**, 10, 11.
- [28] Y. Chen, S. Li, X. Pei, J. Zhou, X. Feng, S. Zhang, Y. Cheng, H. Li, R. Han, B. Wang, *Angew. Chem., Int. Ed.* **2016**, 55, 10.
- [29] K. Ma, T. Islamoglu, Z. Chen, P. Li, M. C. Wasson, Y. Chen, Y. Wang, G. W. Peterson, J. H. Xin, O. K. Farha, *J. Am. Chem. Soc.* **2019**, 141, 15626.
- [30] D. Klemm, B. Heublein, H.-P. Fink, A. Bohn, *Angew. Chem., Int. Ed.* **2015**, 54, 9029.
- [31] H. Cheng, L. Lijie, B. Wang, X. Feng, Z. Mao, G. J. Vancso, X. Sui, *Prog. Polym. Sci.* **2020**, 106, 101253.
- [32] X.-F. Zhang, Z. Wang, M. Ding, Y. Feng, J. Yao, *J. Mater. Chem.* **2021**, 9, 23353.
- [33] J. Nie, H. Xie, M. Zhang, J. Liang, S. Nie, W. Han, *Carbohydr. Polym.* **2020**, 250, 116955.
- [34] P. Küsgens, S. Siegle, S. Kaskel, *Adv. Eng. Mater.* **2009**, 11, 93.
- [35] B. Zhang, H. Chen, Q. Hu, L. Jiang, Y. Shen, D. Zhao, Z. Zhou, *Adv. Funct. Mater.* **2021**, 31, 2105395.
- [36] S. Mintova, V. Valtchev, *Zeolites* **1995**, 16, 31.
- [37] M. A. Hubbe, R. A. Gill, *BioResources* **2016**, 11, 2886.
- [38] H. Katsuzawa, N. Kinoshita, H. Shouji, M. Odagiri, H. Zang, *J. Fiber Soc. Japan.* **1994**, 50, 452.
- [39] B. Thomas, M. C. Raj, A. K. B, R. M. H, J. Joy, A. Moores, G. L. Drisko, C. Sanchez, *Chem. Rev.* **2018**, 118, 11575.
- [40] R. J. Moon, A. Martini, J. Nairn, J. Simonsen, J. Youngblood, *Chem. Soc. Rev.* **2011**, 40, 3941.
- [41] B. D. Mattos, B. L. Tardy, L. G. Greca, T. Kämäräinen, W. Xiang, O. Cusola, W. L. E. Magalhães, O. J. Rojas, *Sci. Adv.* **2020**, 6, 19.
- [42] D. Klemm, F. Kramer, S. Moritz, T. Lindström, M. Ankerfors, D. Gray, A. Dorris, *Angew. Chem., Int. Ed.* **2011**, 50, 5438.
- [43] M. F. F. Pego, M. L. Bianchi, P. K. Yasumura, P. K. Yasumura, *Wood Sci. Technol.* **2020**, 54, 1587.
- [44] G. Fathi, J. E. Kasmani, *BioResources* **2019**, 14, 2798.
- [45] A. Sobhan, K. Muthukumarappan, Z. Cen, L. Wei, *Carbohydr. Polym.* **2019**, 225, 115189.
- [46] Z. Wang, M. Li, X.-F. Zhang, Y. Zhou, J. Yao, *Cellulose* **2022**, 29, 1873.
- [47] Z. Zhang, N. Ma, S. Yao, W. Han, X. Li, H. Chang, Y.-Y. Wang, *ACS Sustainable Chem. Eng.* **2021**, 9, 5827.
- [48] M. Matsumoto, T. Kitaoka, *Adv. Mater.* **2016**, 28, 1765.
- [49] S.-C. Li, B.-C. Hu, L.-M. Shang, T. Ma, C. Li, H.-W. Liang, S.-H. Yu, *Adv. Mater.* **2022**, 34, 2202504.
- [50] N. Keshavarzi, F. Mashayekhy Rad, A. Mace, F. Ansari, F. Akhtar, U. Nilsson, L. Berglund, L. Bergström, *ACS Appl. Mater. Interfaces* **2015**, 7, 14254.
- [51] L. T. Gibson, C. M. Watt, *Corros. Sci.* **2010**, 52, 172.
- [52] S. Bette, G. Eggert, A. Fischer, J. Stelzner, R. E. Dinnebier, *Corros. Sci.* **2018**, 132, 68.
- [53] P. Horcajada, S. Surblé, C. Serre, D.-Y. Hong, Y.-K. Seo, J.-S. Chang, J.-M. Grenèche, I. Margiolaki, G. Férey, *Chem. Commun.* **2007**, 27, 2820.
- [54] S. Wuttke, A. Zimpel, T. Bein, S. Braig, K. Stoiber, A. Vollmar, D. Vollmar, D. Müller, K. Haastert-Talini, J. Schaeske, M. Stiesch, G. Zahn, A. Mohmeyer, P. Behrens, O. Eickelberg, D. A. Bölükbas, S. Meiners, *Adv. Healthcare Mater.* **2017**, 6, 1600818.

- [55] M. I. Severino, A. Al Mohtar, C. Vieira Soares, C. Freitas, N. Sadovnik, S. Nandi, G. Mouchaham, V. Pimenta, F. Nouar, M. Daturi, G. Maurin, M. L. Pinto, C. Serre, *Angew. Chem., Int. Ed.* **2023**, 62, e202211583.
- [56] A. Permyakova, S. Wang, E. Courbon, F. Nouar, N. Heymans, P. D'ans, N. Barrier, P. Billemont, G. De Weireld, N. Steunou, M. Frère, C. Serre, *J. Mater. Chem.* **2017**, 5, 12889.
- [57] Y.-K. Seo, J. W. Yoon, J. S. Lee, Y. K. Hwang, C.-H. Jun, J.-S. Chang, S. Wuttke, P. Bazin, A. Vimont, M. Daturi, S. Bourrelly, P. L. Llewellyn, P. Horcajada, C. Serre, G. Férey, *Adv. Mater.* **2012**, 24, 806.
- [58] M. Tong, D. Liu, Q. Yang, S. Devautour-Vinot, G. Maurin, C. Zhong, *J. Mater. Chem.* **2013**, 1, 8534.
- [59] G. Gnanasekaran, A. G. Y. S. Mok, *Sep. Purif. Technol.* **2021**, 277, 119655.
- [60] A. Dhakshinamoorthy, M. Alvaro, P. Horcajada, E. Gibson, M. Vishnuvarthan, A. Vimont, J.-M. Grenèche, C. Serre, M. Daturi, H. Garcia, *ACS Catal.* **2012**, 2, 2060.
- [61] S. Wuttke, P. Bazin, A. Vimont, C. Serre, Y.-K. Seo, Y. K. Hwang, J.-S. Chang, G. Férey, M. Daturi, *Chemistry* **2012**, 18, 11959.
- [62] E. Soubeyrand-Lenoir, C. Vagner, J. W. Yoon, P. Bazin, F. Ragon, Y. K. Hwang, C. Serre, J.-S. Chang, P. L. Llewellyn, *J. Am. Chem. Soc.* **2012**, 134, 10174.
- [63] J. W. Yoon, Y.-K. Seo, Y. K. Hwang, J.-S. Chang, H. Leclerc, S. Wuttke, P. Bazin, A. Vimont, M. Daturi, E. Bloch, P. L. Llewellyn, C. Serre, P. Horcajada, J.-M. Grenèche, A. E. Rodrigues, G. Férey, *Angew. Chem., Int. Ed.* **2010**, 49, 5949.
- [64] P. Horcajada, C. Serre, M. Vallet-Regí, M. Sebban, F. Taulelle, G. Férey, *Angew. Chem., Int. Ed.* **2006**, 118, 6120.
- [65] S. Sene, M. T. Marcos-Almaraz, N. Menguy, J. Scola, J. Volatron, R. Rouland, J.-M. Grenèche, S. Miraux, C. Menet, N. Guillou, F. Gazeau, C. Serre, P. Horcajada, N. Steunou, *Chem.* **2017**, 3, P303.
- [66] M. Giménez-Marqués, A. Santiago-Portillo, S. Navalón, M. Álvaro, V. Briois, F. Nouar, H. Garcia, C. Serre, *J. Mater. Chem.* **2019**, 7, 20285.
- [67] F. Nouar, M. Manchal, M. Benzaqui, N. Steunou, M. Gimenez-Marques, S. Sene, C. Serre, European patent application 17305119.4, **2017**.
- [68] E. J. Foster, R. J. Moon, U. P. Agarwal, M. J. Bortner, J. Bras, S. Camarero-Espinosa, K. J. Chan, M. J. D. Clift, E. D. Cranston, S. J. Eichhorn, D. M. Fox, W. Y. Hamad, L. Heux, B. Jean, M. Korey, W. Nieh, K. J. Ong, M. S. Reid, S. Renneckar, R. Roberts, J. A. Shatkin, J. Simonsen, K. Stinson-Bagby, N. Wanasekara, J. Youngblood, *Chem. Soc. Rev.* **2018**, 47, 2609.
- [69] Y.-K. Seo, J. W. Yoon, J. S. Lee, U.-H. Lee, Y. K. Hwang, C.-H. Jun, P. Horcajada, C. Serre, J.-S. Chang, *Microporous Mesoporous Mater.* **2012**, 157, 137.
- [70] E. Abraham, B. Deepa, L. A. Pothan, M. Jacob, S. Thomas, U. Cvelbar, R. Anandjiwala, *Carbohydr. Polym.* **2011**, 86, 1468.
- [71] J. Zhao, W. Zhang, X. Zhang, X. Zhang, C. Lu, Y. Deng, *Carbohydr. Polym.* **2013**, 97, 695.
- [72] E. Oliaei, P. A. Lindén, Q. Wu, F. Berthold, L. Berglund, T. Lindström, *Cellulose* **2020**, 27, 2325.
- [73] E. Bellido, M. Guillevic, T. Hidalgo, M. J. Santander-Ortega, C. Serre, P. Horcajada, *Langmuir* **2014**, 30, 5911.
- [74] O. Soubélet, M. A. Presta, M. Marx-Figini, *Die Makromol. Chem.* **1989**, 190, 3251.
- [75] T. P. Nevell, *Cellulose Chem and its Applications*, (Ed: T. P. Nevell), Ellis Horwood, **1985**.
- [76] E. Kontturi, A. Meriluoto, P. A. Penttilä, N. Baccile, J.-M. Malho, A. Potthast, T. Rosenau, J. Ruokolainen, R. Serimaa, J. Laine, H. Sixta, *Angew. Chem., Int. Ed.* **2016**, 55, 14455.
- [77] N. Gurnagul, D. H. Page, M. G. Paice, *Nord. Pulp Pap. Res. J.* **1992**, 311992, 152.
- [78] J. Tétreault, P. Bégin, S. Paris-Lacombe, A.-L. Dupont, *Lignocellulose* **2019**, 26, 2013.
- [79] M. I. Severino, A. Al Mohtar, C. V. Soares, O. Kolmykov, C. Freitas, I. Dovgaliuk, C. Martineau, V. Pimenta, F. Nouar, G. Maurin, M. L. Pinto, C. Serre, *J Mater Chem* **2023**, 11, 4238.
- [80] J. Kammer, F. Truong, C. Boissard, A.-L. Soulié, A.-L. Dupont, L. Simon, V. Gros, B. Lavédrine, *J. Cultural Heritage.* **2021**, 47, 50.
- [81] K. Dedecker, R. S. Pillai, F. Nouar, J. Pires, N. Steunou, E. Dumas, G. Maurin, C. Serre, M. L. Pinto, *ACS Appl Mater Interfaces* **2018**, 10, 13886.